SEARCHING FOR DARK MATTER IN SPACE

A. Morselli
INFN Roma II and Dept. of Physics, University of Roma "Tor Vergata"

Abstract

Experimental cosmology has been steadily progressing over the last few years. The emerging picture is of a cosmological average matter density of $\Omega_m = 0.27 \pm 0.04$ which is much larger than the baryon density $\Omega_b = 0.044 \pm 0.004$. The nature of the astronomical dark matter is still unresolved. The favoured candidate for the nonbaryonic component is a neutral weakly-interacting massive particle (WIMPs) with a mass in the range from tens of GeV to TeV. They would naturally appear as one of the thermal leftovers from the early Universe and their existence is predicted in several classes of extensions of the Standard Model of particle physics. The most popular case is that of the lightest neutralino in R-parity conserving supersymmetric models. Considerable effort has been put into the search for dark matter WIMPs in the last decade, with several complementary techniques applied. One route worth being explored is provided by indirect signatures. Neutralinos should pervade the Milky Way halo and be concentrated at the galactic centre and in the cores of the sun and earth. As they mutually annihilate, they should produce high energy photons and antimatter cosmic-rays and should therefore generate spectral distortions in the corresponding backgrounds. The direct detection of annihilation products in cosmic rays offers an alternative way to search for supersymmetric dark matter particles candidates. The study of the spectrum of gamma-rays, antiprotons and positrons in space has already showed some deviation from the expected signals but with weak statistical evidence. We will review the present situation and the achievable limits with the experiments PAMELA and GLAST.

1 Propagation of Cosmic Rays in the Milky Way and Its Uncertainties

The key problem in the quest for exotic signals in cosmic rays is to know the standard contributions.

The most complete equation for the propagation of cosmic rays that includes all the known physical processes is

$$\begin{aligned}\frac{\partial\psi(\mathbf{r},p,t)}{\partial t} &= q(\mathbf{r},p)+\nabla\cdot(D_{xx}\nabla\psi-\mathbf{V}_c\psi)+\frac{d}{dp}\,p^2D_{pp}\frac{d}{dp}\,\frac{1}{p^2}\,\psi \\ &- \frac{\partial}{\partial p}\left[\dot{p}\psi-\frac{p}{3}\,(\nabla\cdot\mathbf{V}_c)\psi\right]-\frac{1}{\tau_f}\psi-\frac{1}{\tau_r}\psi\,, \qquad (1)\end{aligned}$$

where $\psi(\mathbf{r},p,t)$ is the total phase space density. We will shortly review here the main features of the physical processes described by this equation implemented in the Galprop code [1, 2].

The second term describes isotropic diffusion, defined by the coefficient that depends on the rigidity (momentum per unit of charge, $\rho = p/Z$)

$$D_{xx} = \beta D_0(\rho/\rho_0)^{\delta}, \qquad (2)$$

inspired by the Kolmogorov spectrum ($\delta = 1/3$) of the weak magnetohydrodynamic turbulence. In [3] was first shown that the Kolmogorov spectrum best reproduces the sharp peak in B/C data. The convection velocity field $\mathbf{V}_c$, that corresponds to the Galactic wind, has a cylindrical symmetry. Its z-component is the only one different from zero. It increases linearly with the distance z from the Galactic plane. This is in agreement with magnetohydrodynamical models [4]. In the Galactic plane there should be no discontinuity in the convection velocity field and so we considered only $V_c(z = 0) = 0$. Reacceleration is determined by the diffusion coefficient in the momentum space D_{pp}. D_{pp} is a function of the corresponding configuration space diffusion coefficient D_{xx} and of the Alfven velocity V_A in the framework of quasi-linear MHD theory [5, 6, 7]

$$D_{pp}(D_{xx},V_A) = \frac{4p^2{V_A}^2}{3\delta(4-\delta^2)(4-\delta)w}\,, \qquad (3)$$

where w characterizes the level of turbulence, and it is equal to the ratio of MHD wave energy density to magnetic field energy density. It is assumed $w = 1$, but the only relevant quantity is V_A^2/w.

The unknown values of parameters such as the Alfven velocity, the convection velocity gradient in Milky Way and the height of the galactic

halo can be constrained by the B/C data. With the sets of the constrained parameters one can find all the possible spectra for the others cosmic rays. This procedure was already used in [8] for another propagation code

Injected spectra of all primary nuclei are power laws

$$dq(p)/dp \propto p^{-\gamma}, \tag{4}$$

where the value of γ can, in principle, vary with species. This power law approximation as well as a small break in the injection indexes γ is allowed in the framework of diffusive shock acceleration models [9, 10, 11].

Source term $q(\mathbf{r}, p)$ for secondaries contains cross sections for their production from progenitors on H and He targets

$$q(\vec{r}, p) = \beta c\, \psi_p(\vec{r}, p)[\sigma_H^{ps}(p) n_H(\vec{r}) + \sigma_{He}^{ps}(p) n_{He}(\vec{r})], \tag{5}$$

where $\sigma_H^{ps}(p)$ and $\sigma_{He}^{ps}(p)$ are the production cross sections for the secondary from the progenitor on H and He targets, ψ_p is the progenitor density, and n_H, n_{He} are the interstellar hydrogen and helium number densities.

The last two terms in equation (1) are loss terms with characteristic times for fragmentation and radioactive decay.

The heliospheric modulation of the local interstellar spectra in the vicinity of the Earth and in the heliosphere hole has to be taken into account in order to obtain the realistic cosmic rays spectra in locations where they are/will be measured (balloon-born or satellite-borne experiments).

We made use of a widely used and tested model in which the transport equation is solved in the force field approximation [12, 13]. That equation describes diffusion processes in the heliosphere and includes effects of heliospheric magnetic field and solar wind. In this case, solar modulation is a function of just a single parameter that describes the strength of the modulation. All the dynamical processes are simulated simply changing the interstellar spectra during the propagation inside the heliosphere:

$$\frac{\Phi^{toa}(E^{toa})}{\Phi^{is}(E^{is})} = (\frac{p^{toa}}{p^{is}})^2, \tag{6}$$

$$E^{is} - E^{toa} = |Ze|\phi, \tag{7}$$

where E and p are energies and momenta of the interstellar and top of the atmosphere fluxes and ϕ is the unique parameter that determines the solar modulation.

In Galprop the model of the Galaxy is three dimensional with cylindrical symmetry; the coordinates are (R, z, p), where R is Galactocentric radius, z is the distance from the Galactic plane, and p is the total particle momentum. The distance from the Sun to the Galactic centre is taken to be 8.5 Kpc. The

propagation region is bounded fixing $R_{max} \equiv R = 30$ Kpc and $z_{max} \equiv z$ beyond which free escape is assumed. The distribution of cosmic rays sources is chosen to reproduce (after propagation) the cosmic rays distribution determined by the analysis of EGRET gamma-ray data done in [11]. The code first computes propagation of primaries, giving the primary distribution as a function of (R, z, p). Then the secondary source function is obtained from the gas density and cross sections. Finally, the secondary propagation is computed.

Secondary to primary CR ratios are the most sensitive quantities on variation of the propagation parameters. This can be verified numerically. Primary to primary and secondary to secondary ratios are not very sensitive to changes in the propagation parameters because they have similar propagation mechanisms. The most accurately measured secondary to primary ratio is boron to carbon ratio (B/C, see [14]). Boron is secondary while, one of its progenitors, carbon is primary. The B/C data are used also because they have relatively well known cross sections. To estimate the quality of the data fit we used the standard χ^2 test

$$\chi^2 = \frac{1}{N-1} \sum_n \frac{1}{(\sigma_n^{B/C})^2} (\Phi_{n,exp}^{B/C} - \Phi_{n,teo}^{B/C})^2, \tag{8}$$

where $\sigma^{B/C}$ are statistical errors for $N = 46$ experimental points and $\Phi_{exp}^{B/C}$ are measured and $\Phi_{teo}^{B/C}$ are predicted values of the ratio.

We analized only the two extreme cases of the propagation models either without convection or without reacceleration. We did not succeed in obtaining satisfactory models with all the physical processes switched on. A possible explanation is that one of the processes is really subdominant in the Galaxy in such a way that the data require either reacceleration or convection to be well fitted. So in the first case we included diffusive and reacceleration effects (see equation (1) and we considered two sub-cases: (DR) without a break in the index of primary injection spectra and (DRB) with a break at the rigidity ρ^γ. The second case (DC) contains diffusion and convection terms from the same equation (1). In this model there are two breaks: one in the index of the primary injection spectra and the other in the spectra of the diffusion coefficient D_{xx}. The first break means that at some rigidity ρ^γ the index γ suffers a discontinuity (see equation (4) and ref. [10] for details), while the second one means that at some rigidity ρ_0 the diffusion index δ suffers a discontinuity (see equation (2) and discussion in ref. [2]).

For the DR model we chose to vary the following parameters: the height of the Galactic halo z, the constant in the diffusion coefficient D_0 (from equation (2)), the index of the diffusion coefficient δ (from the same equation), the primary spectra injection index γ for all the energies (from equation (4)) and the Alfven velocity v_A that determines the strength of reacceleration. In

order to find the allowed range of these parameters we have required a reduced χ^2 less than 2 for the fit of the B/C experimental data [14]. In figure 1 are presented the enveloping curves of all the good fits with solid lines around the best fit line for the same model, that is represented with dashed line. We took the experimental data with relatively small solar modulation parameter ϕ between 325 MV and 600 MV, where the force field approximation is better justified than for the high modulation parameters. The allowed ranges of propagation parameters of this model are given in the table 2. In the case

Table 1: Allowed values for diffusion and convection (DC) model parameters.

par./val.	$z[Kpc]$	$D_0[\frac{cm^2}{s}]$	δ_2	$\frac{dV_C}{dz}[\frac{Km}{skpc}]$	γ_1	γ_2
minimal	3.0	$2.3\ 10^{28}$	0.48	5.0	2.42	2.14
best fit	4.0	$2.5\ 10^{28}$	0.55	6.0	2.48	2.20
maximal	5.0	$2.7\ 10^{28}$	0.62	7.0	2.50	2.22

Table 2: Allowed values for diffusion and reacceleration (DR) model parameters.

par./val.	$z[Kpc]$	$D_0[cm^2s^{-1}]$	δ	γ	$v_A[Kms^{-1}]$
minimal	3.0	$5.2\ 10^{28}$	0.25	2.35	22
best fit	4.0	$5.8\ 10^{28}$	0.29	2.47	26
maximal	5.0	$6.7\ 10^{28}$	0.36	2.52	35

Table 3: Allowed values for DRB parameters.

par./val.	$z[Kpc]$	$D_0[\frac{cm^2}{s}]$	δ	γ_1	γ_2	$v_A[\frac{Km}{s}]$
minimal	3.5	$5.9\ 10^{28}$	0.28	1.88	2.36	25
best fit	4.0	$6.1\ 10^{28}$	0.34	1.92	2.42	32
maximal	4.5	$6.3\ 10^{28}$	0.36	2.02	2.50	33

of the DC model we chose to vary the following parameters: D_0, the diffusion index δ_1 below the reference rigidity $\rho_0 = 4$ GV and δ_2 above it (all those parameters are from equation (2)), the halo size z, the convection velocity V_c (from equation (1)) and the injection index for primary nuclei γ_1 below the reference rigidity $\rho_0^\gamma = 20$ GV and γ_2 above it (see equation (4)). Enveloping curves of B/C fits for the reduced χ^2 values less than 2.8 are given in figure 1.

Positive variations around $\delta_1 = 0$ gave unsatisfactory fit. In order to take the smallest possible break of this index we decided not to take negative δ_1 values. Allowed values for the propagation parameters can be found in table 1.

We found the spectra that correspond to the parameters of the best fit of B/C data for subFe/Fe ratio (see figure 2), protons, helium and electrons as well as the corresponding propagation parameters uncertainties. For DC model the obtained fits are good, while DR overestimates protons (figure 3), helium (figure 4) and electrons.

In order to improve those fits, we considered the DR model with a break in the injection index for the primary nuclei spectra with a rigidity of 10 GV [2, 10]. We determined the allowed values of the propagation parameters (table 3) demanding the same reduced χ^2=2 as for DR model (see figure 1). The positron and antiproton uncertainties are presented in figure 6. Even if positrons at low energies and protons and helium in all the energy range are fitted better (see figure 3 and figure 4), they remain overestimated. For the computation of B/C ratio, Galprop uses only one principal progenitor and compute weighted cross sections. Introducing the break in the index of the primary injection spectra in DR model give worst electron data fit than in the case without the break. On the other side, the antiproton spectra remain unchanged, still significantly and systematically underestimated in all the energy range.

We also calculated how the antiproton spectra change on variation of the most important antiproton production cross sections. Antiprotons are created in the interactions of primary cosmic rays (protons and other nuclei) with interstellar gas. Dominant processes are interactions of high energy primary protons with hydrogen, $p + p \rightarrow p + p + p + \bar{p}$. Parameterization of this cross section is given in [17]. Other cross sections, those of primary protons with other nuclei, are studied in reference [18]. From these, the most important are those that involve helium, and they contribute less than 20% of the total production of all the antiprotons. All the heavier nuclei together give just a few percents of the total production.

Uncertainties of cross sections influence the antiproton spectra uncertainties from 20% up to 25% depending on energy and the uncertainty in the measurements of helium to hydrogen ratio bring another 3% to 7%, depending on energy.

Total uncertainties of positrons and antiprotons are presented in figure 6. They vary from 35% up to 55% for antiprotons and from 20% up to 40% for positrons for both the models in the current experimental data energy range.

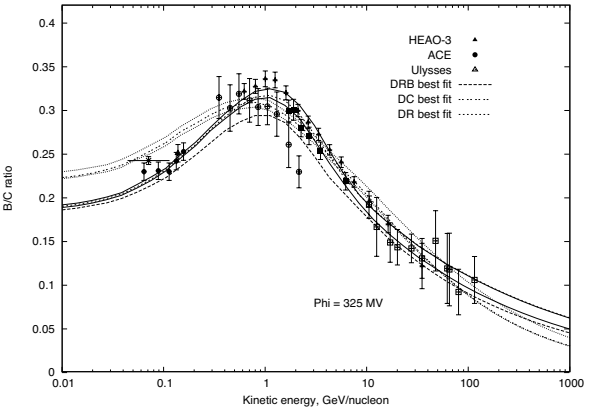

Figure 1: Propagation parameters uncertainty for B/C ratio: for DR model is given with solid lines around the best fit (dashed line), while for DC model is given with dotted lines around the best fit (dashed line). For DRB model we give the best fit (dashed line). For the complete list of the experimental data see [14].

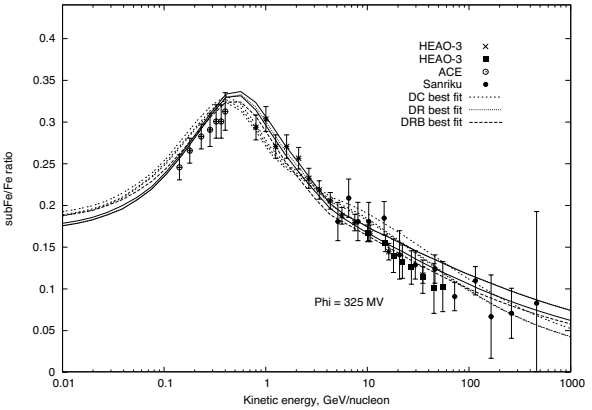

Figure 2: Ratio (Sc+Ti+V)/Fe that corresponds to the propagation parameters that give the best fits of B/C data for the DC model is given with dashed line and it is inside the corresponding uncertainty band given with dashed lines. The ratio for the DR model is given with dotted line and it is inside the uncertainty given with solid lines, while for DRB model is given with larger-step dashed line without the uncertainty band around. Experimental data are taken from [16].

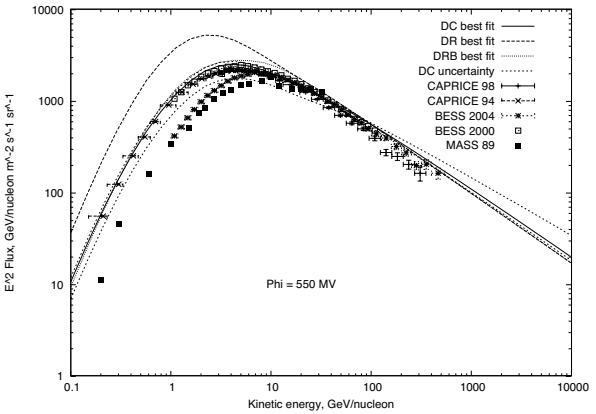

Figure 3: Upper and lower bounds of proton spectra due to the uncertainties of the propagation parameters for the DC model are represented with dashed lines. Spectra that correspond to the parameters of the best B/C fit are given for the DC model with solid line, for the DR model with dashed line and for the DRB model with dotted line. Experimental data are taken from [15].

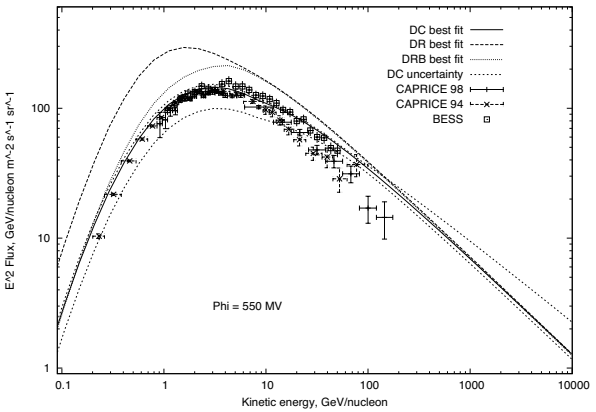

Figure 4: Upper and lower bounds of helium spectra due to the uncertainties of the propagation parameters for the DC model are represented with dashed lines. Spectra that correspond to the parameters of the best B/C fit are given for the DC model with solid line, for the DR model with dashed line and for the DRB model with dotted line. Experimental data are taken from [15].

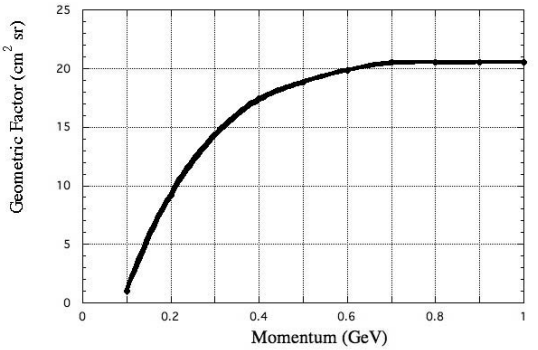

Figure 5: Geometric factor of PAMELA

2 Component of the Antiproton Spectra Induced by Neutralino Annihilations

In this section we take into account the possibility of a neutralino induced component in the $\bar{p}$ flux. Our analysis is performed in the well known mSUGRA framework [19] with the usual gaugino mass universality at the grand unification scale M_{GUT}.

In the general framework of the minimal supersymmetric extension of the Standard Model (MSSM), the lightest neutralino is the lightest mass eigenstate obtained from the superposition of four interaction eigenstates, the supersymmetric partners of the neutral gauge bosons (the bino and the wino) and Higgs bosons (two Higgsinos). Its mass, composition and couplings with Standard Model particles and other superpartners are functions of several free parameters one needs to introduce to define such supersymmetric extension. In the mSUGRA model, universality at the grand unification scale is imposed. With this assumption the number of free parameters is limited to five

$$m_{1/2},\ \ m_0,\ \ sign(\mu),\ \ A_0 \ \text{ and } \ \tan\beta\,,$$

where m_0 is the common scalar mass, $m_{1/2}$ is the common gaugino mass and A_0 is the proportionality factor between the supersymmetry breaking trilinear couplings and the Yukawa couplings. $\tan\beta$ denotes the ratio of the VEV-s of the two neutral components of the SU(2) Higgs doublet, while the Higgs mixing μ is determined (up to a sign) by imposing the Electro-Weak Symmetry Breaking (EWSB) conditions at the weak scale. In this context the MSSM can be regarded as an effective low energy theory. The parameters at the weak

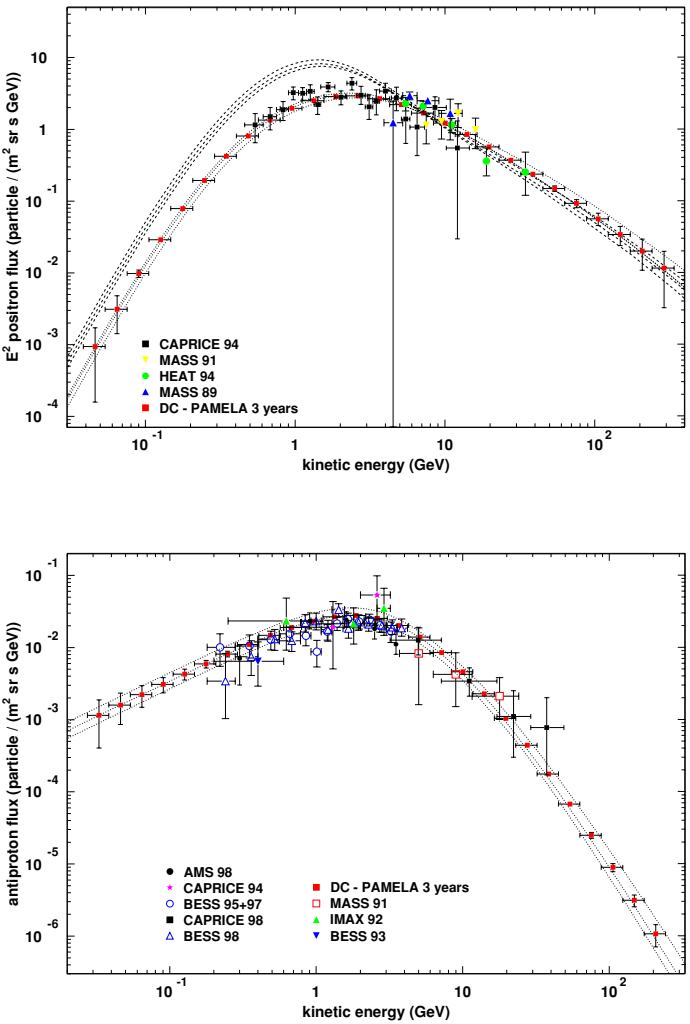

Figure 6: Experimental data (from [32]) confronted with PAMELA's expectations for positrons (top) and antiprotons (bottom) for DC model background. Total uncertainties and the spectra that correspond to the parameters of the best B/C fit for DC model are given with dotted lines while for DRB model with dashed lines.

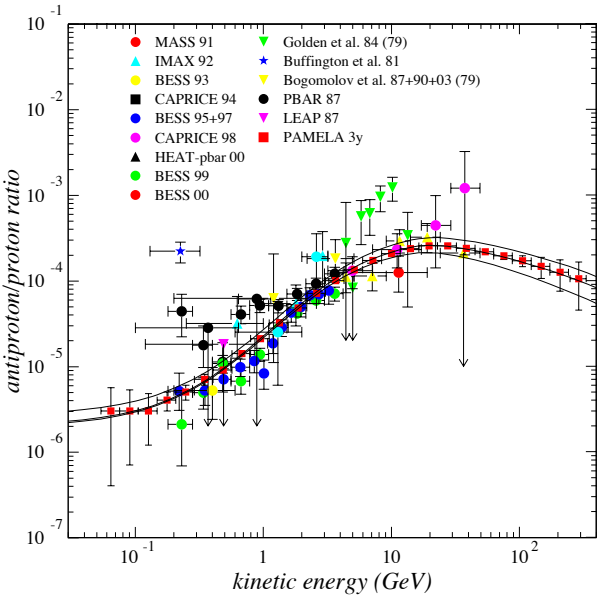

Figure 7: Experimental data (from [32]) confronted with PAMELA's expectations for the antiproton proton ratio for the DC model background. The propagation uncertainty band of the antiproton proton ratio and the curve that corresponds to the parameters of the best B/C fit in the middle are given with solid lines.

energy scale are determined by the evolution of those at the unification scale, according to the renormalization group equations (RGEs) [20].

For this purpose, we have made use of the ISASUGRA RGE package in the ISAJET 7.64 software [21]. After fixing the five mSUGRA parameters at the unification scale, we extract from the ISASUGRA output the weak-scale supersymmetric mass spectrum and the relative mixings. Cases in which the lightest neutralino is not the lightest supersymmetric particle or there is no radiative EWSB are disregarded.

The ISASUGRA output is then used as an input in the DarkSUSY package [22]. The latter is exploited to:

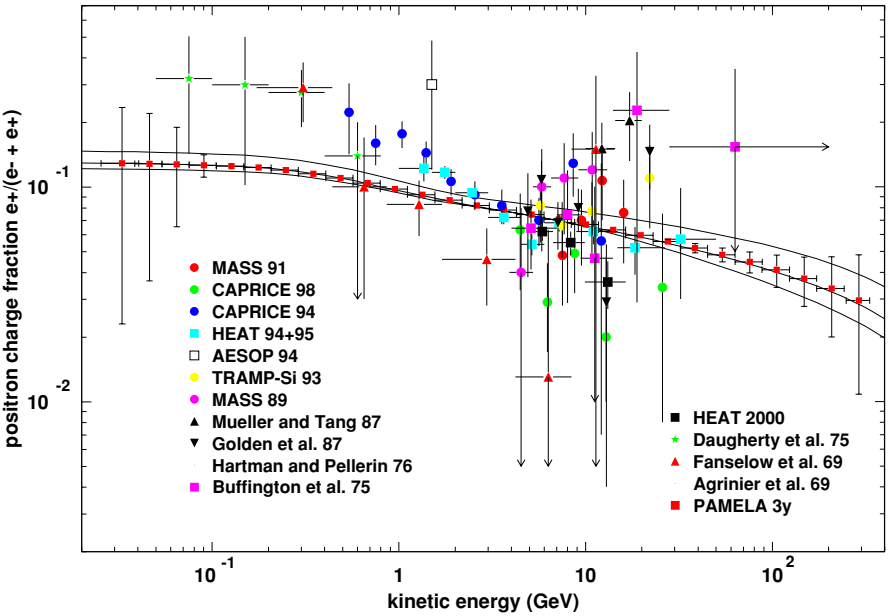

Figure 8: Experimental data (from [32]) confronted with PAMELA's expectations for positron charge fraction for the DC model background. The propagation uncertainty band of the positron charge fraction and the curve that corresponds to the parameters of the best B/C fit in the middle are given for a better comparison.

- reject models which violate limits recommended by the Particle Data Group 2002 (PDG) [23];
- compute the neutralino relic abundance, with full numerical solution of the density evolution equation including resonances, threshold effects and all possible coannihilation processes [24];
- compute the neutralino annihilation rate at zero temperature in all kinematically allowed tree-level final states (including fermions, gauge bosons and Higgs bosons);
- DarkSUSYestimates the induced antiproton yield by linking to the results

of the simulations performed with the Lund Monte Carlo program Pythia [25].

This setup as well as some other similar scenarios were already considered in the context of dark matter detection and of an improvement of the cosmic rays data fits (a list of references includes, for example [26, 27]).

2.1 Clumpy Halo Models

In order to obtain a higher antiproton flux in the case of high neutralino masses we assumed a small clump scenario [28] for the dark matter halo in our Galaxy. In fact, in equation (10) the dependence of the antiproton flux is $\propto \rho^2/m_\chi^2$: without increasing the total halo mass by increasing the average density, there can be assumed a local density enhancement, that will also lead to the increasing of the antiproton flux.

By hypothesis the clump is a spherical symmetric compact object with mass M_{cl} and some density profile $\rho_{cl}\left(\vec{r}_{cl}\right)$. We denote with f the dark matter fraction concentrated in clumps and we introduce the dimensionless parameter d

$$d = \frac{1}{\rho_0} \frac{\int d^3 r_{\rm cl} \left[\rho_{\rm cl}\left(\vec{r}_{\rm cl}\right)\right]^2}{\int d^3 r_{\rm cl} \rho_{\rm cl}\left(\vec{r}_{\rm cl}\right)} \tag{9}$$

that gives the overdensity due to a clump with respect to the local halo density $\rho_0 = \rho(r_0)$, where r_0 is our distance from the Galactic Center (GC). In a smooth halo scenario the total neutralino induced $\bar{p}$ flux calculated for $r = r_o$ is given by [29]

$$\Phi_{\bar{p}}(r_0, T) \equiv (\sigma_{\rm ann} v) \sum_f \frac{dN^f}{dT} B^f \left(\frac{\rho_0}{m_{\tilde{\chi}}}\right)^2 C_{\rm prop}(T) \; . \tag{10}$$

where T is the $\bar{p}$ kinetic energy, $\sigma_{\rm ann} v$ is the total annihilation cross section times the relative velocity, m_χ is the neutralino mass, B^f and dN^f/dT, respectively, the branching ratio and the number of $\bar{p}$ produced in each annihilation channel f per unit energy and $C_{\rm prop}(T)$ is a function entirely determined by the propagation model. In the presence of many small clumps the $\bar{p}$ flux is given by

$$\Phi_{\bar{p}}^{\rm clumpy}(r_0, T) = f d \cdot \Phi_{\bar{p}}(r_0, T) \tag{11}$$

For the smooth profile we assumed a Navarro, Frenck and White profile (NFW) [30].

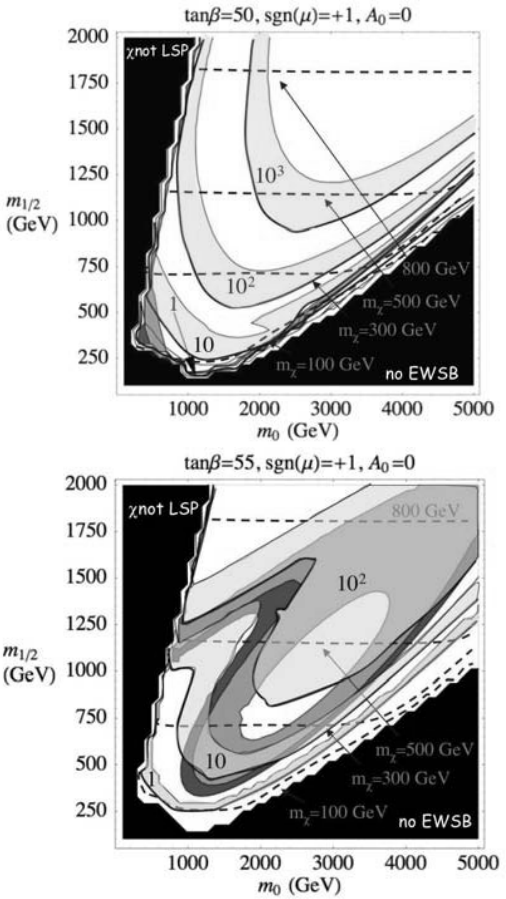

Figure 9: Contour plots for the minimum fd needed for a PAMELA disentanglement (upper bounds of the translucent bands) and for the maximum fd allowed by current experimental data (lower bounds of the translucent bands). In the upper panel $\tan\beta = 50$ while in the lower panel $\tan\beta = 55$. The other parameters (keep fixed) are $A_0 = 0$ and $sgn(\mu)$=1. Black color represents the regions in the parameter space that are excluded either by accelerator bounds or because electroweak symmetry breaking is not achieved or because the neutralino is not the lightest supersymmetric particle. Red (dark shaded) are domains with Ωh^2 in the WMAP region $0.09 < \Omega h^2 < 0.13$, while green (light shaded) are the parameter space domains with $0.13 < \Omega h^2 < 0.3$. We also show the equi-neutralino mass contours (blue dashed lines).

2.2 Propagation of the Neutralino Induced Component

The primary contribution to the antiproton flux is computed using the public code DarkSUSY [31]. We modified the antiproton propagation in order to be consistent with the DC propagation model as implemented in Galprop code. We assumed diffusion coefficient spectra used in Galprop code with our best fit values for the diffusion constants D_0 and δ. In DarkSUSY, the convection velocity field is constant in the upper and the lower Galactic hemispheres (with opposite signs, and so it suffers unnatural discontinuity in the Galactic plane), while Galprop uses magnetohydrodynamically induced model, in which one component of velocity field along the Galactic latitude (the only one that is different from zero) increases linearly with the Galactic latitude [4]. We assumed an averaged convection velocity calculated from the Galactic plane up to the Galactic halo height z.

2.3 Detection of the Secondary Components in the Positron and the Antiproton Fluxes by PAMELA

In this section we calculate the statistical errors for the PAMELA [32] experiment for the positron and the antiproton background spectra calculated with Galprop [1].

The calculation is done for a three years mission assuming the geometric factor given in figure 5. PAMELA's statistical errors for positrons and antiprotons in the case of the DC model are given in figure 6. In figures 7 and 8 there are the PAMELA expectations together with the propagation uncertainties for the antiproton proton ratio and positron charge fraction respectively.

3 The Possibility of Disentanglement of the Neutralino Induced Component in the Antiproton Flux With PAMELA

In this section we present the results we found about the minimal values of the clumpiness factors fd needed to disentangle a neutralino induced component in the antiproton flux with PAMELA. We computed this factor as a function of the mSUGRA parameters, fixing A_0, $\tan\beta$ and $\mathrm{sign}(\mu) = 1$. In this way the clumpiness factor become a function of m_0 and $m_{1/2}$ parameters. Similar analysis were already made in the literature (see for example [27]).

For the discrimination we requested the following conditions:

[1]The list of the people and the institutions involved in the collaboration together with the on-line status of the project is available at *http://wizard.roma2.infn.it/*.

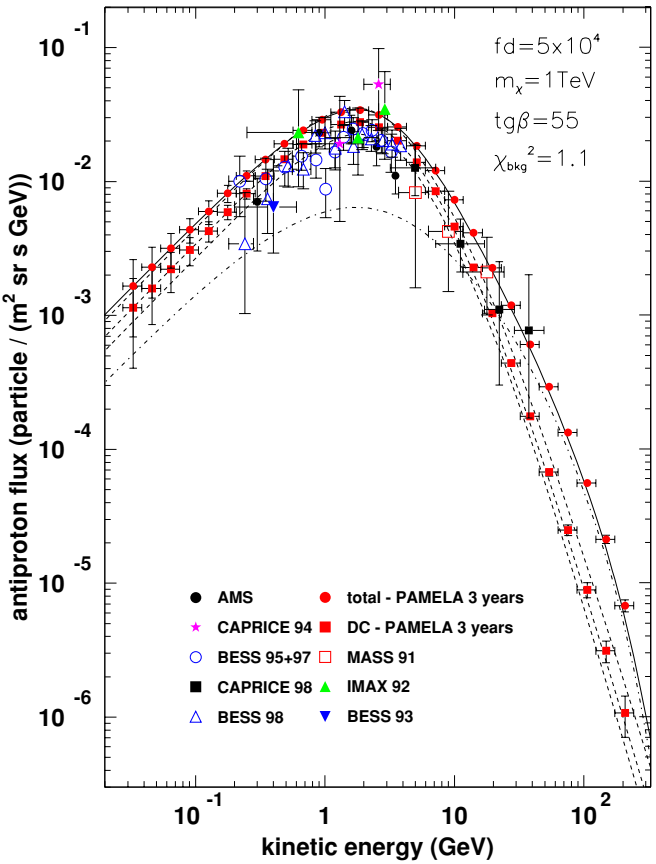

Figure 10: Antiproton absolute flux: theoretical predictions for total uncertainty and best B/C fit for DC model (dashed lines) . Experimental data are from [9]. The PAMELA expectations points (red squares) for DC background are for three years of data taking. The dash-dotted line is a neutralino induced contribution for a neutralino mass of 1 TeV (see text) and a clumpiness factor fd of 5 10^4while the solid line is total contribution calculated with the addition of the DC background and the red circles are the corresponding PAMELA points.

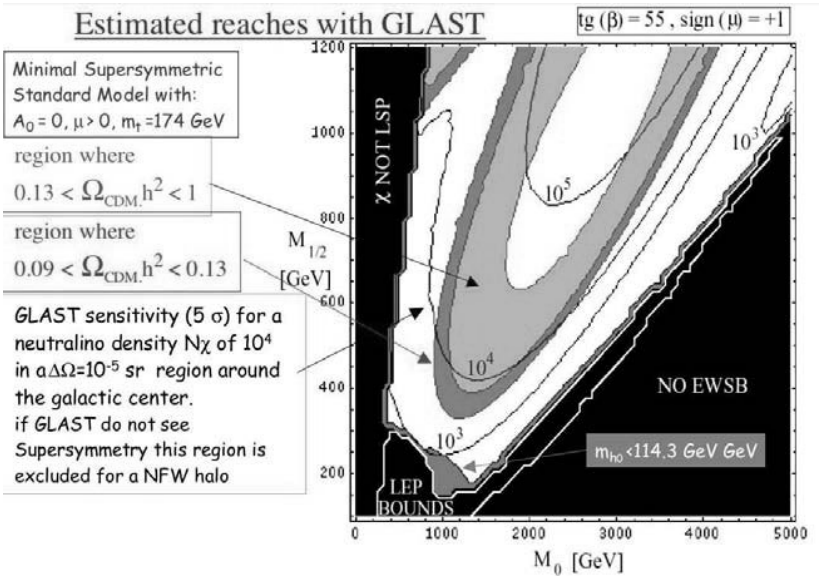

Figure 11: Contour plot in the mSUGRA $(m_0, m_{1/2})$ plane, for the value of the normalization factor N_χ, that allows the detection of the neutralino γ ray signal with GLAST. In the green region $0.13 \leq \Omega_\chi h^2 \leq 1$, while the red region corresponds to the WMAP range $0.09 \leq \Omega_\chi h^2 \leq 0.13$. The black region corresponds to models that are excluded either by incorrect EWSB, LEP bounds violations or because the neutralino is not the LSP. In the dark shaded region $m_{h_0} < 114.3$ GeV and h_0 is the lightest Higgs.

1. The total antiproton flux $\phi_{tot} = \phi_{bkg} + \phi_{susy}$ gives a good fit of the experimental data.

2. Difference between ϕ_{tot} and DC model ϕ_{bkg} is detectable by PAMELA.

The first condition is satisfied if

$$\chi^2_{fit} = \frac{1}{N-1} \sum_n \frac{(\Phi_n^{exp} - \Phi_n^{tot})^2}{(\sigma_n^{exp})^2} \tag{12}$$

is less than the $\chi^2_{fit,0} = 1.7$, for $N = 40$ experimental points. The second condition is satisfied if

$$\chi^2_{discr} = \frac{1}{M-1} \sum_m \frac{(\Phi_m^{bkg} - \Phi_m^{tot})^2}{(\sigma_m^{P,bkg})^2} \tag{13}$$

is greather than the $\chi^2_{discr,0} = 1.8$, for $M = 29$ points, where $\sigma_m^{P,bkg}$ are the PAMELA statistical errors associated to the background flux (those presented in figure 6).

Figure 10 shows an example of good model satisfing both conditions. The SUSY contribution to the $\bar{p}$ flux is for a neutralino mass of 1 TeV (obtained from a particular choice of mSUGRA parameters) and a clumpiness factor fd of $5\ 10^4$. Higher neutralino masses improve high energy data fit but only with the increase of the clumpiness factor because of the dependence from the inverse neutralino mass squared m_χ in the $\bar{p}$ flux.

For each model we found the minimal value of the clumpiness factor fd needed to satisfy both conditions. As the clumpiness factor is a function of m_0 and $m_{1/2}$ parameters we made contour plots calculating equi-clumpiness factors lines. The results for $\tan\beta$=50 and $\tan\beta$=55 is presented in figure 9. The regions in parameter space that are excluded either by accelerator bounds or because electroweak symmetry breaking is not achieved or because the neutralino is not the lightest supersymmetric particle are represented with black color. Red (dark shaded) color indicates the (m_0, $m_{1/2}$) domains with Ωh^2 in the WMAP [33] region $0.09 < \Omega h^2 < 0.13$. Green (light shaded) color indicates the parameter space regions with values of $0.13 < \Omega h^2 < 0.3$. In figures 9 the equi-clumpiness factors lines for the maximal allowed (by the present experimental data) fd are represented by the lower bound of the translucent light blue (very light shaded) regions.The translucent regions denote the parameter space domains that correspond to models that satisfy both the conditions (12) and (13), keeping fixed values of fd (those indicated inside the regions).

It can be seen that even small clumpiness factors (of order 10) are sufficient for PAMELA detection. This is very important, because, even if we consider a DC model as the background flux (that alone already gives a good fit of the experimental data) it is still possible to disentangle a supersymmetric component in a wide region of the parameter space (in comparison with the WMAP allowed zone). For higher value of $\tan\beta$ the situation is even more favourable [35].

The search for supersymmetric signal with PAMELA will be complementary to the search for neutralinos looking at the distortion of the gamma-ray flux that will be performed with GLAST.

Figure 11 show the GLAST capability for $\tan\beta$=55 to probe in two years the supersymmetric dark matter hypothesis [20]. The figures show in the $(m_0, m_{\frac{1}{2}})$ plane, the iso-contour regions for the minimum allowed value of the neutralino density in a $\Delta\Omega = 10^{-5} sr$ region around the galactic center. The density depends from the halo shape of the neutralino distribution, that is still matter of debate and can vary from a value of $N_\chi = 3 \times 10^1$ for an

isotermal profile up to $N_\chi = 10^4$ for a NFW profile [30] and up to $N_\chi = 10^7$ for a Moore profile [36]. GLAST indeed can explore a good portion of the supersymmetric parameter space especially at large values of $\tan\beta$ and if the halo has a NFW (or steeper) profile. This is a very steep ($1/r$) profile but consistent with available dynamical constraints on the Galaxy [20].

References

1. Strong A W and Moskalenko I V 1998 *ApJ* **509** 212
   Moskalenko I V and Strong A W 1998 *ApJ* **493** 694-707
2. Moskalenko I V, Strong A W, Ormes et al. 2002 *ApJ* **565** 280
3. Heinbach U and Simon M 1995 *ApJ* **441** 209-221
4. Zirakashvili V N, Breitschwerdt D, Ptuskin V S and Volk H J 1996 *A&A* **311** 113
5. Fermi E 1949 *Phys. Rev.* **75** 1169
6. Seo E S and Ptuskin V S 1994 *ApJ* **431** 705
7. Berezinskii V S, Bulanov S V, Dogiel V A, Ginzburg V L, Ptuskin V S 1990 *Astrophysics of Cosmic Rays* (North Holland, Amsterdam)
8. Donato F et al. 2001 *ApJ* **536** 172
   Donato F, et al. 2003 *Phys. Rev. D* **69** 06350
9. Blandford R D and Ostriker J P 1980 *ApJ* **237** 793
10. Ellison D C et al. 2001 *ApJ* **563** 191-201
11. Strong A W and Mattox J R 1996 *A & A* **308** L21
12. Gleeson L J and Axford W I 1968 *ApJ* **154** 1011
13. Perko J S 1987 *A&A* **184** 119
14. Davis A J et al. 2000 *AIP Conf. Proc. 528, ed. Mewaldtet R A al* (AIP, New York)
    Lukasiak A et al. 1999 *Proc. 26th Int. Cosmic-Ray Conf.* (Salt Lake City) **3** 41
15. Boezio M et al. 2003 *Astroparticle Physics* **19** 583-604
16. Davis A J et al. 2000 *On the low energy decrease in Galactic cosmic ray Proc ACE-2000 Symp.* ed. Mewald R A et al. (NY: AIP) AIP Conf. Proc. **528** 421-424

17. Tan L C and Ng L K 1983 *J. Phys. G* **9** 227

18. Gaisser T K and Schaefer R K 1992 *ApJ* **394** 174

19. Hall L J, Lykken J, and Weinberg S 1983 *Phys. Rev. D* **27** 2359

20. Cesarini A, Fucito F, Lionetto A, Morselli A and Ullio P 2004 *Astropart. Phys.* **21** 267

21. Baer H, Paige F E, Protopopescu S D and Tata X *Preprint* hep-ph/0001086

22. Gondolo P, et al. 2004 *JCAP* **07** 008 *Preprint* astro-ph/0211238

23. Hagiwara K et al. 2002 *Phys. Rev.* **D66** 010001

24. Edsjo J, Schelke M, Ullio P and Gondolo P 2003 *JCAP* **04** 001

25. Sjöstrand T 1994 *Comp. Phys. Comm.* **82** 74

26. Feng J L, Matchev K T and Wilczek F 2001 *Phys. Rev. D* **63** 045024
Bottino A, et al. 2001 *Phys. Rev.* **D63** 125003
Ellis J, Ferstl A and Olive K A 2002 *Phys. Lett.* **B532** 318
Bertin V, Nezri E and Orloff J 2002 *Eur. Phys. J.* **C26** 111

27. Profumo S and Ullio P 2004 *JCAP* **07** 006
Bottino A et al. 2004 *Phys. Rev. D* **69** 063501
de Boer W et al. 2003 *Preprint* IEKP-KA/2003-17, [hep-ph/0309029]

28. Bergstrom L, Edsjö J, Gondolo P and Ullio P 1999 *Phys. Rev. D* **59** 043506

29. Bergstrom L, Edsjo J and Ullio P Bergstrom L, Edsjo J, Ullio P 1999 *ApJ* **526** 215 [astro-ph/9902012]

30. Navarro J F, Frenk C S and White S D M 1996 *ApJ* **462** 563

31. Gondolo P, Edsjo J, Ullio P, Bergstrom L, Schelke M and Baltz E A 2004 *JCAP* **07** 008

32. Picozza P and Morselli A 2003 *J. Phys. G: Nucl. Part. Phys* **29** 903-911

33. Bennet C L et al. 2003 *ApJ Suppl.* **148** 1

34. Chan K L, Chattopadhyay U, Nath P 1997 *Phys. Rev. D* **58** 096004
Feng J L, Matchev K T, Moroi T 2000 *Phys. Rev. D* **61** 075005
Baer H et al. 2003 *J. High Energy Phys.* **0306** 054

35. A.M.Lionetto, A.Morselli, V.Zdravkovic, astro-ph/0502406 submitted to JCAP

36. S. Ghigna et al., Astrophys. J. **544** (2000) 616.